Journal of Aeronautics & Aerospace Engineering

Mazzola et al., J Aeronaut Aerospace Eng 2017, 6:1
DOI: 10.4172/2168-9792.1000182

Research Article Open Access

Development and Technological Characterization of Multi-functional Aeronautical Coating From Lab-Scale to the Relevant Environment

Mazzola L[1]*, Bruno G[1], Galasso B[1], Quaranta V[1], Albano F[1], Auletta A[1] and Coriand L[2]

[1]CIRA - Italian Aerospace Research Centre, Via Maiorise 1, 81043 Capua, Italy
[2]Fraunhofer Institute for Applied Optics and Precision Engineering, Albert-Einstein-Str. 7, 07745 Jena, Germany

Abstract

Ice adhesion on critical aircraft surfaces is a serious potential hazard that runs the risk of causing accidents. Frozen contaminants cause rough and uneven surfaces which will disturb smooth air flow and greatly degrade the ability of the wing to generate lift and increasing drag.

Amongst icing mitigation systems, passive anti-icing coatings represent a challenge to reduce the ice nucleation and growth, reducing the power consumption of the active de-icing systems and consequently the fuel consumption.

In this work the advanced properties and effectiveness of the new multifunctional coating with ice-phobic and aesthetical properties are described. In particular advanced morphological characterizations based on Atomic Force Microscopy and Laser Scanning Microscopy measurements as well as subsequent Power Spectral Density analysis were performed to evaluate the surface roughness.

Contact angle measurements were executed in order to determine the wettability and surface free energy as well as work of adhesion in flight conditions. In addition, dynamic analysis of the impact of single water droplets on the new multifunctional coating and the classical livery coating were performed in order to demonstrate the different physical behavior during the impingement.

It was also demonstrated that the new multifunctional coating overcome the environmental test similarly to the commercial livery coating in accordance with the aeronautical specification.

Finally, two NACA symmetric airfoils were design and developed using 3D printing technology. The surfaces were coated with a commercial coating in one case and with the new multifunctional coating in the other case. Both airfoils were tested in the Icing Wind Tunnel at different conditions in order to evaluate the effectiveness, in terms of reduction of accreted ice, of the new multifunctional coating respect to the commercial one. Tests demonstrated the reduction of accreted ice of 50% using the new multifunctional coating.

Keywords: Icephobic coating; 3D printing; Icing wind tunnel; Unmanned Air Vehicle (UAV); Roughness; PSD function; FEM analysis; Environmental tests

Introduction

De-icing on the ground is usually done by spraying aircraft with a de-icing fluid based on ethylene glycol, propylene glycol, diethylene glycol as well as urea and acetates which are toxic or has negative effects for aquatic life [1]. The United States Environmental Protection Agency had estimated that before 1990, U.S. airports had discharged approximately 28 million gallons, 50% glycol solutions, of aircraft deicing fluids annually to receiving waters. As of 2000, the discharges have been reduced to 21 million gallons of de-icing and anti-icing fluids (50% concentration) per year to receiving waters with an additional 2 million gallons discharged to publically owned treatment works [2]. The used de-icing fluid during daily operations at the airport can contribute as a source of air, water and soil pollution. Additionally, these operations can adversely affect the climatic conditions, plants, buildings and animals [3,4].

An inflight ice protection system on existing aircrafts heat the vulnerable regions using hot air bleed from the engine compressor [4] and/or electrothermal solutions. However, the air-bleed reduces the efficiency of the engines and the pipe network for the hot air bleed adds considerable weight and maintenance requirements. Another established approach is to use pneumatic bladders in vulnerable regions which can be inflated to detach ice from these critical locations. There is then a risk of impacting other parts of the aircraft structure or being ingested by the powerplants, damaging fan blades. Due to weight and maintenance implications, anti-icing and de-icing systems are restricted to specific, albeit critical, regions and so ice can still accumulate at other sections of the lifting surface [5]. The current anti-icing and de-icing system will build up weight, increase fuel consumption and add complexity to the aircraft systems. A Passive Ice Protection System (PIPS) and mixed passive / active methods could significantly reduce aircraft fuel consumption. The aim is to improve the power efficiency and operational effectiveness of the current anti-icing or de-icing system in an environmentally friendly way [6-12].

Studies on passive anti-icing systems such as icephobic coating are actually ongoing because even if, in literature [13-27], there are several formulations with superhydrophobic and icephobic properties, they are not really applicable in aeronautics. Mainly this is due to the following criticisms:

***Corresponding author:** Mazzola L, CIRA - Italian Aerospace Research Centre, Via Maiorise 1, 81043 Capua, Italy, Tel: +39 0823623153; E-mail: l.mazzola@cira.it

Received December 21, 2016; **Accepted** January 04, 2017; **Published** January 08, 2017

Citation: Mazzola L, Bruno G, Galasso B, Quaranta V, Albano F, et al. (2017) Development and Technological Characterization of Multi-functional Aeronautical Coating From Lab-Scale to the Relevant Environment. J Aeronaut Aerospace Eng 6: 182. doi: 10.4172/2168-9792.1000182

- The new icephobic formulations must be applied on top of the component. Therefore in case of aircraft components, it will be applied over the livery coating altering the aesthetical aspect.
- Difficulties of the production at the industrial scale and following insertion in the actual production chain.
- They must be cost effective.
- They are eco-friendly according to the REACh regulations and VOC free.
- They must overcome all aeronautical specifications (Airbus, Boeing, Bombardier, Embraer, etc…) and the relative standard tests.

For this reason the development of a multifunctional coating with combined aesthetical and icephobic properties represents a product really challenge.

In the previous work Mazzola [28] designed and realized a new polymeric formulation for aerospace applications. In fact the efficacy of the icephobic properties at lab scale (having also aesthetical properties) was demonstrated as well as a complete physical, chemical morphological and mechanical characterizations were performed.

This work describes the advances in the development of the new formulation of this multifunctional coating. In particular, the surface structure at micro and nanoscale was investigated through atomic force microscopy as well as laser scanning microscopy and compared with SEM micrographs. For a complete understanding of the surface roughness and its influence on the wetting and icing behavior respectively, a semi-empirical approach consisting of Power Spectral Density analysis procedure and a subsequently derived universal structural parameter were utilized. This so-called wetting parameter is directly connected to the contact angle and, hence, enables an estimation of the wetting behavior of a specific surface structure. Or, as for this research, the other way around: If different wetting behavior or specific ones occur, then the question about the cause arises. This mainly concerns the roughness of a surface that, besides chemical composition, essentially governs its wetting properties [29,30].

Environmental test was performed in order to evaluate the durability of both coatings in harsh conditions (high percentage of relative humiditiy for a long time).

In addition dynamic tests of water droplet impingement at lab scale were performed in order to study the impact of small supercooled water droplets on the new icephobic surface.

All of these experiments were useful to understand the properties and the real behavior of the new multifunctional icephobic coating. Using all of these experimental data (i.e. the surface free energy and wettability of the new coating), a FEM numerical simulation was performed in order to study the reduction of adhesion between ice and the new multifunctional icephobic coating.

Starting from TRL 2 in the previous work [28], the advances on the characterization of the new multifunctional coating at lab scale, along with the availability of new 3D printing technology and Icing Wind Tunnel facility, allowed to reach to this new multifunctional coating, TRL 5 (relevant environment).

Materials and Methods

Materials

The new ice-phobic coating was obtained starting from the commercial coating used as livery, i.e. a matt grey livery coating. Once that the substrate was scraped with P400 sandpaper and washed, an epoxy-modified polyamide primer using VOC (Volatile Organic Compounds) exempt solvents (solvent based High Solid coating) was applied in order to improve the adhesion of the topcoat, inhibit the corrosion and level the surface.

Above the primer, a water-based 3-component, isocyanate cured polyurethane topcoat (in accordance to Registration, Evaluation, Authorization and Restriction of Chemicals- REACH regulation). The formulation of the topcoat was modified in order to give further functionality, such as ice-phobicity without alter the aesthetical properties and the other mechanical and corrosive properties. Both coatings were deposited through spray process on substrate of CFRP composites (Carbon Fiber Reinforced Polymer) because this type of application is addressed mainly for Unmanned Air Vehicle (UAV) that is usually realized in composite materials.

The temperature of the substrate was 20°C during the spray process. The dimension of the spray nozzle was 1.2 mm, the temperature of the air carrier was 20°C and the air-pressure was 2 bar. The drying of the coatings was realized using a drying chamber at temperature of 120°C.

Physical and chemical characterization

In order to replicate the same thermodynamic conditions of flight, it is necessary to change both temperature and pressure. As known the surface free energy may be defined as the increase in Gibbs free energy of the whole system per unit increase in interfacial area, carried out under conditions of constant temperature and pressure that is [31]:

$$\gamma = \left(\frac{\Delta G}{\Delta A}\right)_{T,p} \quad (1)$$

Contact angle changes in case the component works at ambient pressure and temperature, at flight temperature and ambient pressure, or at temperature and pressure in flight. Aiming at a replication of the flight conditions, a test room, to mount on a classical contact angle measurement instrument, was designed and developed at CIRA [28]. In this work, a new version of the test room is described. In fact the main limitation of the first version of the test room was mainly the supplying and use of pellets of dry ice (Carbon Dioxide). To overcome this limitation the new version of the test room uses a Ranque-Hilsch Vortex Tube – RHVT powered by the line of compressed air. In this way, utilizing this system, it is possible to reach temperature out of the cold side of the RHVT temperature of -70°C.

The new test room was realized in insulator material (in particular top, bottom and two lateral and parallel surfaces), such as polycarbonate with a thickness of 2 mm, whereas the other two lateral and parallel surfaces were realized in aluminum Al2024-T6 with a thickness of 1 mm.

Polycarbonate was chosen because, other than thermal insulating, it is also transparent. This property is needed to capture the liquid drops applied on the surface with the camera of the contact angle instrument. The two lateral and parallel surfaces were realized in Aluminum where one was isolated using Polystyrene whereas the other was used for the heat exchange.

On the external surface of this last Aluminum surface was a cooling chamber of polystyrene mounted, on which the cold side of RHVT is connected. In this way the cold air exits from the RHVT and it come into contact with the Aluminum surface for the heat exchange. The

holes present on the sides of the cooling chamber were used to let out the cold air produced by RHVT.

Using this method it is possible to reach temperature of -50°C in the test room. The temperature within the test room was detected using a thermocouple K-type.

The top surface of the test room has a hole with an elastic membrane in order to allow the insertion of the syringe needle to deposit the liquid drop. The syringe employed was Hamilton 600 series – 5 µl.

Supercooled water droplets were realized using a microliter syringe of Hamilton. Once reached the temperature and pressure in the test room, a small quantity of bi-distilled water was sucked up within the capillary of the needle. Afterwards, the needle was inserted through the elastic membrane of the test room and leaved within the room for 30 seconds, in order to reduce the temperature of the water from ambient temperature to near zero Celsius degree. After this time, the water droplet was deposited very slowly on the surface of the sample presents on the bottom of the test room. During the deposition, the water droplet had a further drastically reduction of temperature; Before reaching the surface of the sample, The droplet becomes supercooled. This supercooled property was simulated with a model of the heat exchange surface and phase shift of the water considering the main characteristics of the water droplet. In order to have the same flight altitude pressure, a circuit with a Venturi tube model (ZH-05-DS-06-06-06) was realized [28].

With this new tool it is possible to replicate the pressure and temperature until a flight altitude of about 16000 meters. According to the standard certification (FAR CS-25 – appendix C), the highest probability to have icing phenomena is 5000 meters, where the temperature is about -12/-15°C and pressure is about 0.5 bar. Note that the test room could be mounted on a micrometric sample-holder, which can be moved on three axes and in addition it is possible to tilt the entire test room in order to determine the advancing and receding contact angle as well as the roll-off angle.

Bi-distilled water, methylene iodide and formamide were used to determine surface free energy and its components, together with the adhesion work and other performance indexes, i.e. advancing and receding contact angle, hysteresis, roll-off angle. During the test, 10 drops (with volume smaller than 3 µl) of each liquid were deposited on the sample surface. The surface free energy was calculated according to the Owens-Wendt method [32]. The Owens-Wendt approach is one of the most commonly used methods for calculating the surface free energy of the materials [33]. The principal assumption of the Owens-Wendt method is that the surface free energy is the sum of the two components: dispersion and polar components [34].

The Owens-Wendt model is represented by the geometric mean relationship:

$$\frac{1}{2}(1+\cos\theta)\gamma_L = \left(\gamma_S^D \cdot \gamma_1^D\right)^{\frac{1}{2}} + \left(\gamma_S^P \cdot \gamma_1^P\right)^{\frac{1}{2}} \quad (2)$$

Where θ is the contact angle between the liquid droplet and surface, γ_L is the liquid total surface tension, γ_1^P is the dispersion component of liquid surface tension and γ_1^P is the polar component of liquid surface tension.

The unknown terms in the equation (2) are γ_S^P which is the dispersion component of the solid surface free energy and γ_S^P which is the polar component of the solid surface free energy.

The value of total surface free energy of the solid is obtained using the following equation:

$$\gamma_S = \gamma_S^D + \gamma_S^P \quad (3)$$

The surface tension of liquids and its components are taken from literature [35]. However these values are referred to standard conditions of ambient temperature and pressure at sea level.

Using the Karbanda's equation, it is possible to rescale the values of surface tension from temperature point of view:

$$\gamma_{T_2} = \gamma_{T_1}\left(\frac{T_C - T_2}{T_C - T_1}\right)^{1,12} \quad (4)$$

where γ_{T_1} represents the surface tension of liquid at 20°C while T_C represents the critical temperature of the liquid. The critical temperatures of the three liquids are reported in Table 1:

Once rescaled the values from temperature point of view, it is necessary to rescale these new value for the new pressure, using the Laplace equation:

$$\gamma_{p_2} = \gamma_{p_1}\left(1 - \frac{k.p_2}{200}\right) \quad (5)$$

where K is a constant value which is a function of employed liquids. For the liquids employed in these experiments K equal to 2 was used. The calculation of all performance indexes of the instrument were determined using a software, designed and developed at CIRA. This software has all main models present in literature other than Owens-Wendt.

It is evident that, in the real condition, the behavior and dynamics of the interaction between the supercooled liquid dropled and surface are more complex, because the supercooled water droplets impact with high speed on the aircraft components. The dynamics of interaction, happening in a few milliseconds, are in non-equilibrium condition and there are several phenomena that can occur, i.e. infiltration due to the water hammer pressure, instantaneous freezing or rapid rolling of the droplet.

In any case, the characterization technique developed in this work allows studying the ice-phobic surface in static conditions. This represents the worst condition since the supercooled water droplet has a long time to reach the equilibrium state and to freeze on the surface.

To evaluate the behavior of the liquid droplet during the impact on both commercial coating and on the new multifunctional coating, a piezoelectric system for microdroplets dispensing, Microdrop MD-K-130, was used. The instrument is equipped with a high speed camera in order to evaluate the instants during the impact of the single small droplets. It is highlighted that this system produces microdroplets with a diameter between 20 µm and 150 µm. These values are in accordance with the dimension of microdroplets produced by the spray bar system of the Icing Wind Tunnel facility. Tests were performed analyzing the impact of water microdroplets with a diameter of 70 µm that imping the surfaces tilted of 40° respect to the horizontal line.

FEM Analysis to Evaluate the Adhesion at the Coating-Ice Interface

The aim of FEM analysis was focused to evaluate the maximum value of force that cause the debonding at the coating-ice interface both for the new multifunctional coating and for the commercial one.

Critical Temperature (°C)		
Water	**Formamide**	**Diiodomethane**
373.94°C	376.45°C	474.42°C

Table 1: Values of the critical temperature of the three liquids employed.

Virtual Crack Closure Technique analysis (VCCT) was chosen as solver and the software Abaqus was used. In this analysis the experimental values of the work of adhesion (measured previously through contact angle measurement technique) were assigned to coating-ice interface and a displacement was imposed. A pre-existing crack (or debonding) was explicitly included in the finite element mesh. During the simulation, the imposed displacement generates an external work that becomes internal energy released by extending the crack (or debonding). The assumption of the method is that the required work to close or to open the crack over the length Δa (propagation variation of the crack as a result of the increment of applied energy) is equal (Figure 1).

The model is composed by:

1. A composite plate with layup $[45, -45, 0, 90]_{3s}$, 24 plies of 0.186 mm of thickness and dimensions of 100 mm × 100 mm;
2. An ice block of 50 mm × 25 mm × 3 mm.
3. A cohesive zone at the interface with a maximum value of work of adhesion which simulate surface property of the coating.

According to this method, the first line of nodes, at the interface, are not linked in order to create a preexisting crack. Thanks to the imposed displacement, the crack proceeds its propagation until to cover the entire zone of interface. The displacement is constant and tangential to the plate, as shown by yellow arrows in Figure 2a. The bottom of the composite plate is clamped and between ice and plate there are cohesive element for adhesion and a friction coefficient of 0.05.

In the Figure 2b, FEM model is reported with a mesh size of 2 mm. As described above, the initial crack has a depth of 2 mm for all width of the ice block (X-direction).

Environmental Test

Environmental tests in the climatic chamber were performed on the samples with commercial and new multifunctional coatings in order to evaluate the durability. Tests were performed in accordance with the standard AER(EP)M-P-001 and ASTM D2247-15. These standards define the combined environmental conditions of the temperature and humidity and the test duration. The ASTM is a general standard, otherwise the AER(EP)M-P-001 is a standard for aeronautical coating, so the main environmental conditions were taken from this last one.

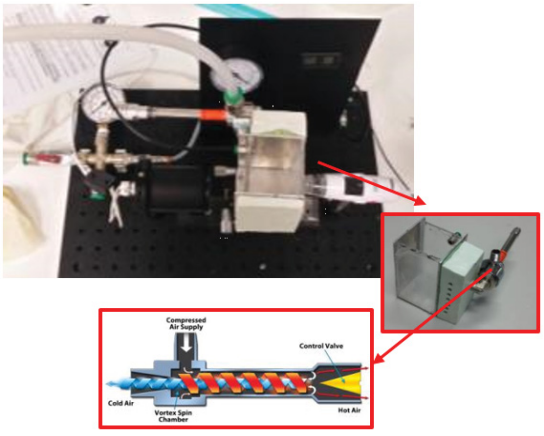

Figure 1: Image of the complete instrument and of the new version of test room. The cold side of the RHVT is connected with the cooling chamber.

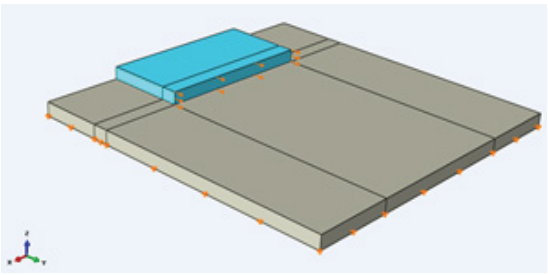

Figure 2a: Boundary condition of the model.

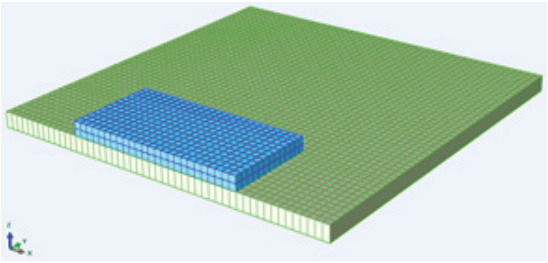

Figure 2b: FEM Model for VCCT analysis.

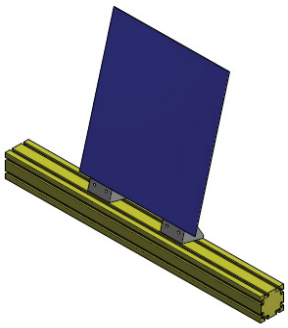

Figure 3: 3D CAD – Axonometric view of sample holder plate.

Tests were performed using the Angelantoni climatic chamber (mod. CH2000). To overcome this test, the coating shouldn't have bubbles, blistering, delaminations and color changes.

For each type of coating, three samples of 150 mm × 80 mm were placed on two sample holder plates tilted of 15° respect to the vertical in accordance with the standard (Figure 3). The process parameters were 38°C of temperature and 100% of relative humidity, test was performed for one month (30 days).

Each week, the test was interrupted for a few minutes in order to oversee and to take a picture of the samples in order to verify if the sample surfaces were degraded, in accordance with the ASTM standard.

The trends of temperature and relative humidity are reported in Figures 4a and 4b.

After the environmental test, several tests on the samples have been carried out with the aim to verify if the environmental condition modified the surface properties of the coating. The first test was the visual inspection of the samples to compare them pre and post-test in order to evaluate blistering or color changes.

The second characterization was performed using optical

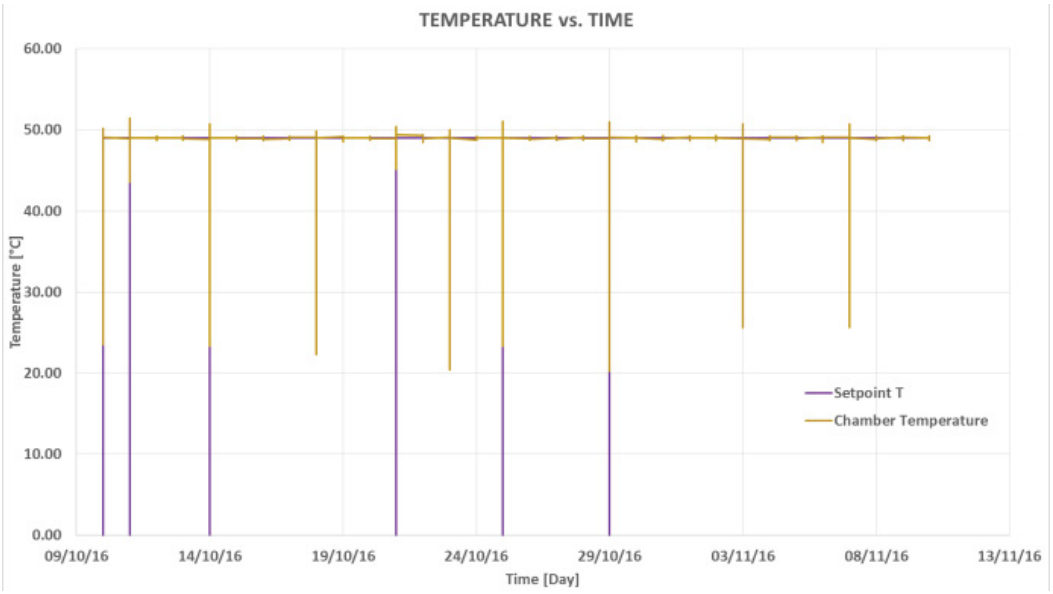

Figure 4a: Test progress of temperature vs. time.

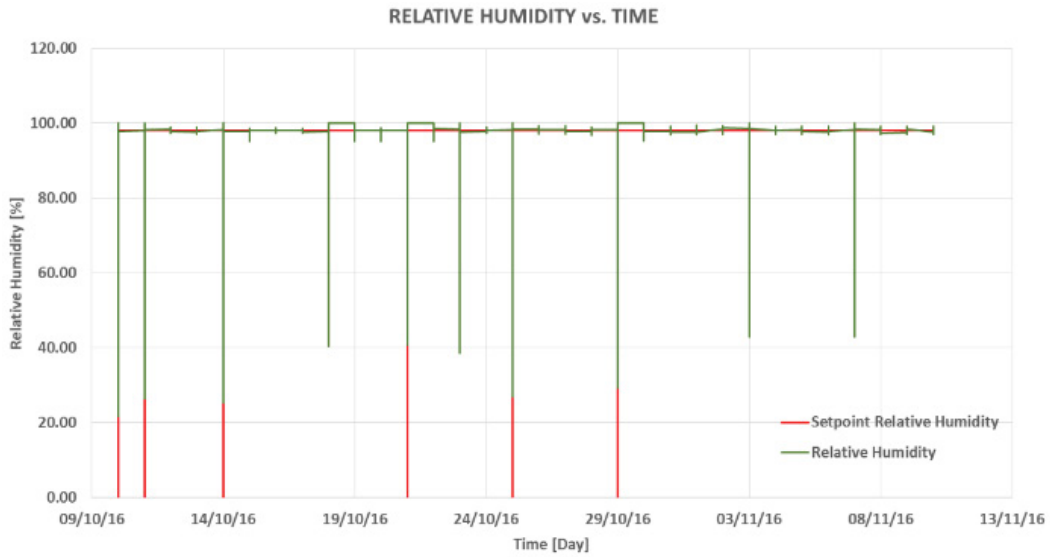

Figure 4b: Test progress of relative humidity vs. time.

microscopy in order to verify uniformity and homogeneity of both coatings and to evaluate in deep blistering or the presence of bubbles. A stereomicroscope Leica MZ12 with camera Leica MC 190 HD was used.

The last test was performed to evaluate the adhesion of the coatings with the substrate. In fact the humidity could infiltrate at the interface between coating and substrate, reducing the adhesion; qualitative adhesion tests were performed in accordance with ASTM D 3359 method B; in particular a cutter PA 2056 (6 teeth – 2.0 mm) and subsequently an adhesive tape PERMACEL #99 were used.

Roughness Analysis

For a robust investigation of the surface morphology and its roughness, atomic force microscopy (AFM) and laser scanning microscopy (LSM) measurements have been performed using a Dimension 3100 AFM from Bruker in the Tapping Mode™ and a LSM 510 from Carl Zeiss Jena GmbH. The vertical resolution of the AFM is limited by the instrumental noise to rms values as low as about 0.04 nm. For the LSM examinations the vertical resolution depends on the objectives (e.g. 100x: rms < 100 nm). For a maximum depth resolution a minimum diameter of the confocal pinhole (10 µm) is used.

To receive quantitative information about the surface roughness, the root mean square (rms) roughness as well as the Power Spectral Density (PSD) function were calculated from the topography data. The rms roughness only considers the vertical dimensions of the surface structure, whereas the PSD function includes the vertical as well as the lateral distribution of surface heights. The PSD can be calculated from surface topography data z(x,y) within a certain scan range L and

afterwards simplified to a 2D-isotropic PSD in case of isotropic surface roughness [29-38]:

$$\mathrm{PSD}(f_x, f_y) = \lim_{x\to\infty} \frac{1}{L^2} \left| \mathrm{FT}\{Z(x,y)\} \right|^2 \quad (6)$$

Using the PSD functions, it is possible to combine the information resulting from the AFM measurements for the higher spatial frequency range and from the LSM measurements for the lower spatial frequency range to analyze the surface roughness within a wide spatial frequency range ($0.01\ \mu m^{-1} \le f \le 1000\ \mu m^{-1}$).

Furthermore, a roughness based structural parameter can be derived from the PSD by means of data reduction procedure. This so-called wetting parameter k_B enables a direct link between the roughness characteristics and the wetting behavior of real surfaces. Thus, it opens up the possibility to separate the influence of roughness properties and chemical material properties on the wettability. For example, previous studies at Fraunhofer IOF [36-38] showed that a κ_B value of at least 0.3 is necessary to reach an extreme wetting behavior like superhydrophobicity. Further information about κ_B as well as an overview of the algorithm for the calculation from PSD data developed at the Fraunhofer IOF are given in [29,30,36].

Design and Production of NACA Airfoils and Deposition of Coatings

In order to evaluate the efficacy of the new multifunctional coating with aesthetical and icephobic properties Icing Wind Tunnel tests were performed. In fact the icephobic and superhydrophobic properties at lab scales in static and dynamic conditions were demonstrated. The following step was to scale up the new formulation of the icephobic coating in relevant environment (reaching Technology Readiness Level 5 – TRL 5).

In order to reach this goal a symmetric NACA 0015 airfoil was design through CAD design using CATIA software. The advantages of utilizing this type of airfoil are mainly due to the absence of the lift (because it is symmetric) and it is enough thick as frontal section area, in order to head-off the supercooled water droplet during the Icing Wind Tunnel tests. The airfoil was designed with respect to achieve a chord length of 100 mm, a wingspan of 150 mm and the height max 15 mm.

Figures 5a and 5b show the CADs of the optimized airfoil and the realized NACA airfoils printed by the 3D printer.

The CAD of NACA airfoil was replicated three times and printed in ABS (Acrylonitrile butadiene styrene) using 3D printer Stratasys Dimension SST-1200ES (Figure 5b).

The three symmetric NACA airfoils were also coated with the commercial coating and the new multifunctional coating. On the third airfoil was applied only the primer to demonstrate the levelling effect of this layer respect to the original roughness of the airfoil (Figure 6a).

Quality control tests were performed in order to confirm the differences in term of contact angles between the two airfoils. As reported in Figure 6b the contact angles were measured at the stagnation point and at the ¼ of chord length. Therefore the two airfoils were ready to be tested in the IWT.

Icing Wind Tunnel Tests

In order to evaluate the efficiency of the icephobic properties of the new multifunctional coating, it was planned to perform comparative tests in an icing facility on both airfoils (equipped with icephobic coating and commercial coating). The aim of the tests was to evaluate the reduction of accreted ice starting from the leading edges without using active de-icing systems.

The tests were performed in the CIRA Icing Wind Tunnel (IWT) facility.

Officially inaugurated in September 2002, the CIRA Icing Wind Tunnel (Figure 7a):

1) It is the largest refrigerated wind tunnel in service;
2) It is the highest speed icing wind tunnel (M=0.7);
3) It is the only facility combining altitude and Temperature simulation;

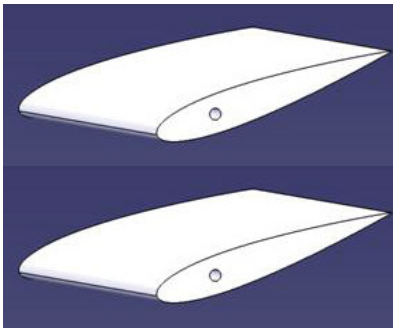

Figure 5a: CAD design of NACA 0015 symmetric air-foil.

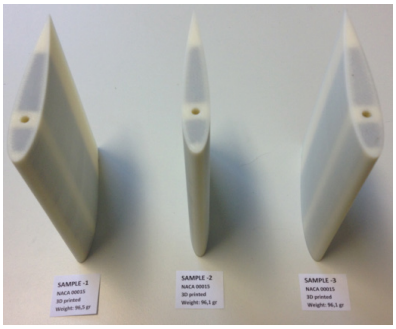

Figure 5b: Three NACA 0015 air-foils printed in ABS using 3D printing technology.

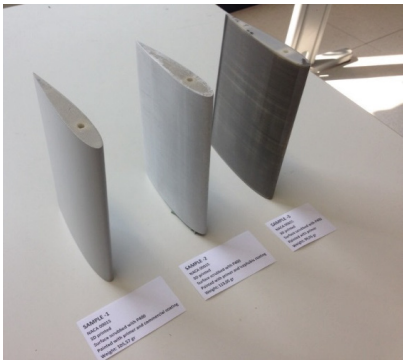

Figure 6a: Three NACA 0015 airfoils coated (from left) with commercial coating, new multifunctional coating and only with primer.

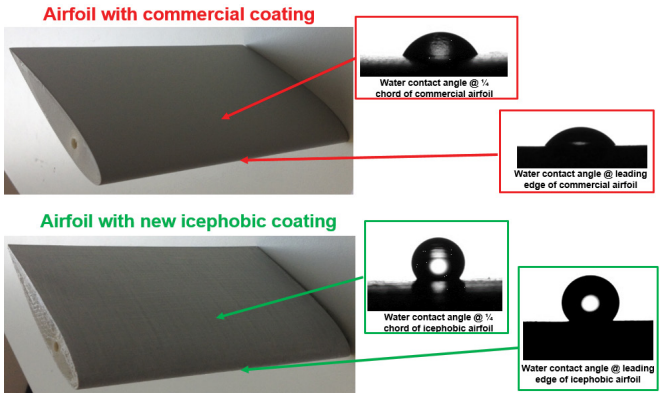

Figure 6b: Quality control test in order to evaluate the wettability property of the two airfoils coated with multifunctional coating and with commercial one.

Figure 7a: CIRA icing wind tunnel.

4) has the largest number of different test sections configurations (4);

5) It has a large number of spray bar nozzles (500) and bars (20);

6) It has the widest operating range for engine flow simulation (1.5-55 kg/s mass flow).

Located in the stilling chamber, the Spray Bar System (SBS) is dedicated to the generation of the icing cloud in all the conditions as prescribed in the current FAR/JAR regulations. Looking at future revisions of the airworthiness regulations, the SBS is also capable to generate Supercooled Large Droplets (SLD) within the range of freezing drizzle conditions.

The extreme values that can be reached in the IWT are the following: temperature simulation down to −40°C, a de-pressurization system for altitude simulation up to 7000 meters (about 23000 feet) and a humidity control down to 70% RH.

The two coated airfoils were installed in the center of the IWT test section as reported in Figure 7b in order to reduce the wall effects, the possible turbulence of the airflow and consequently to have the best distribution of the cloud in terms of cloud uniformity.

Tests were performed according to the FAR-25 appendix C and the test matrix is reported in Table 2.

Where V is the airflow speed, T is the static temperature, h is the altitude, MVD is the water droplet median volumetric diameter, LWC is the Liquid Water Content that measures the concentration of the water in a cloud.

Test 5 was performed in the same tunnel and cloud conditions of Test 1 in order to check the repeatability of the results.

Results

Tests with the new tool were performed both on a classical livery coating and on the new icephobic formulation. In particular ten droplets of each liquid: bidistilled water, di-iodomethane and formamide were deposited on the surfaces in order to determine surface free energy and its components (polar and dispersion components). Tests were performed in standard conditions, i.e. ambient temperature and pressure at sea level, and in simulated flight conditions, i.e. temperature of -12°C and pressure of 0.5 bar. As reported in Figure 8, the great difference between the water contact angle of the commercial coating and the new icephobic formulation is evident.

From Figures 8a and 8b, it is evident that the two samples have the same aesthetical aspect. No differences in terms of color, gloss, brilliance are evident. The two samples seem the same, but, as showed in Figures 8c and 8d, the behavior of the freezed water droplet on the surface is completely different. The commercial coating is hydrophilic, whereas the new formulation has super hydrophobic/icephobic behavior. It is necessary to highlight that this static condition represents the harsh condition in which the coating will work. In fact, as described previously, the coating is under airflow. Therefore the water droplet does not remain on the surface but it rolls away. It is evident that in case of hydrophilic coating, as reported in Figures 8a and 8c, this behavior does not happen; at most it tends to slide away.

In any case, in Figures 8c and 8d the contact angle measurements of the supercooled water droplets applied on both samples are reported. The commercial coating has a water contact angle of about 48°, whereas the new icephobic coating has a water contact angle of about 160°. The improvement of water contact angle was higher than 70%.

Realizing also the contact angle measurements with other two liquids (formamide and diiodomethane), it was possible to determine the surface free energy and other chemical and physical performance indexes.

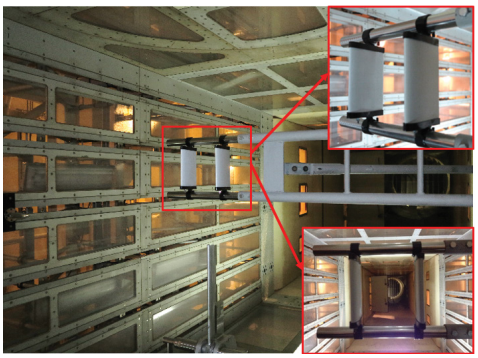

Figure 7b: The two coated air-foils installed in the centre of the IWT test section.

S. No	V [m/s]	T (°C)	h[ft]	MVD [mm]	LWC [g/m³]	Note
Test 1	95	-25	20000	22	0.23	repeatability
Test 2	95	-25	17000	20	0.2	
Test 3	95	-25	5000	19	0.14	
Test 4	95	-25	sea level	25	0.37	
Test 5	95	-25	20000	22	0.23	

Table 2: ITW process parameters.

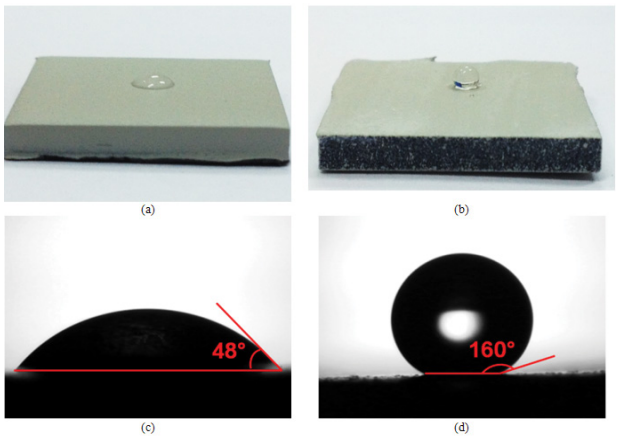

Figure 8: (a) Image of sample with commercial coating. It is evident the freezed water droplet on the surface which spreads on the surface. (b) Image of sample with new icephobic coating. It is evident the freezed water droplet on the surface which assumes a spherical shape on the surface. (c) Micrography obtained during the contact angle measurements in which is evident that the contact angle is under 50° for the commercial coating. (d) Micrography obtained during the contact angle measurements in which is evident that the contact angle is about 160° for the new icephobic coating.

As showed in Figure 9, a drastic reduction of these performance indexes is evident; in fact the surface free energy decrease of the 85%, whereas the dispersion component of the 77% and polar component of 99%. Note that the polar component mainly influences the adhesion between water droplet and the surface, therefore the drastic reduction of this component allows to estimate the reduction of the adhesion of water.

This last statement is also confirmed by the experimental values of work of adhesion. In fact author calculated the work of adhesion of the classical commercial coating and the new icephobic formulation. The reduction of the 92% is evident from Figure 10.

From FEM analysis, a comparative graphic between commercial coating and new multifunctional coating (Figure 11) was obtained. Thanks to the knowledge of the adhesion energies of two coatings, the maximum value of force necessary to debond the ice from the surface coating (in blue the commercial coating and in red new multifunctional coating) was determined. In Figure 11 it is evident that on the surface of the new multifunctional icephobic coating, the required force is about four time lower than the commercial one.

From Figure 12a, it is possible to notice clearly the initial crack in blue, required for the boundary condition of the VCCT method, whereas in Figures 12b and 12c it is evident that two different frames that describe the evolution of the debonding of the ice from the surface coating (in blue the debonding area and in red the adhesive area).

The different behavior of the two coatings is due not only to the different chemical composition of the surface but also to the different morphology of the two coatings. In fact, as showed in Figures 13a-13c at three different magnifications, it is evident that the classical commercial coating shows a smooth surface.

Whereas the new anti-ice formulation shows a surface rougher than the commercial one (Figure 13d). In particular in Figure 13e several micro-features are showed; in addition, improving the magnification on each micro-feature, a nanostructure is evident. A spherical shape roughness is described in Figure 13f.

In addition to the SEM images, Figures 14 and 15 show the topographic images and rms values resulting from AFM and LSM measurements. These results confirm the previous observation: The icephobic sample surface exhibits an obviously higher surface roughness in all investigated measurement fields than the reference

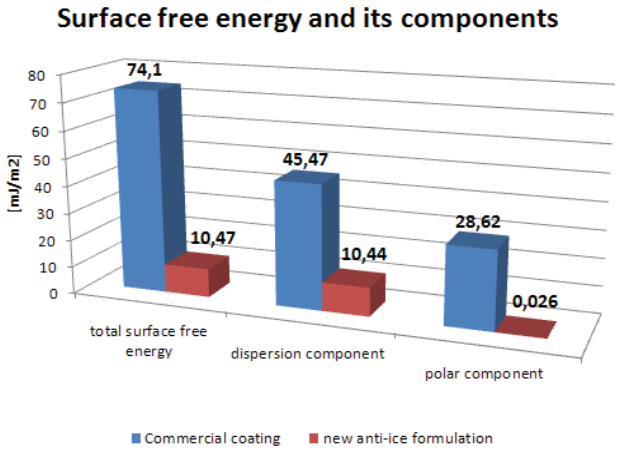

Figure 9: Comparison of the experimental data of the surface free energy and its components both for classical formulation and for the new anti-ice formulation.

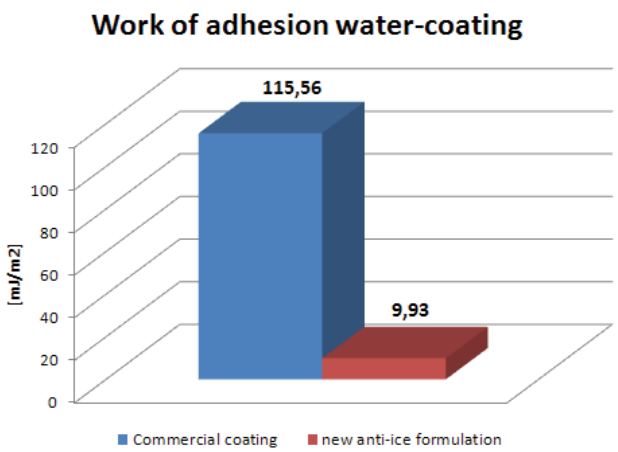

Figure 10: Comparison of the work of adhesion between the classical commercial coating and the new formulation with anti-ice properties.

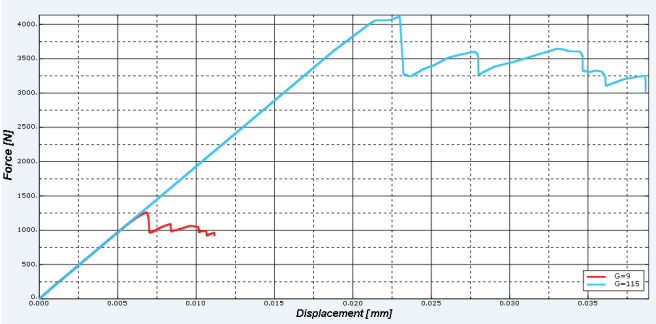

Figure 11: Displacement of commercial coating and new multifunctional coating.

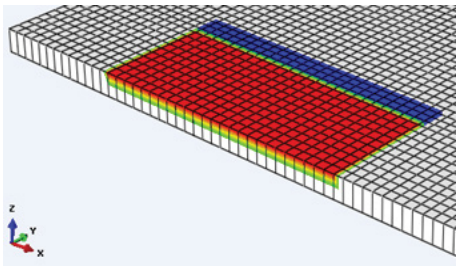

Figure 12a: Detachment before FEM simulation.

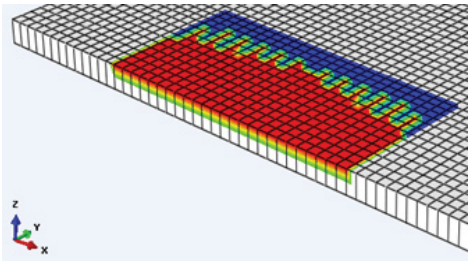

Figure 12b: Advancement of the ice detachment during the FEM simulation.

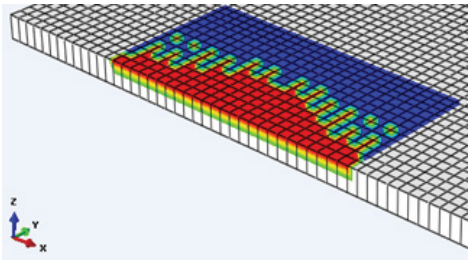

Figure 12c: Advancement of the ice detachment during the FEM simulation.

sample surface. The spherical shape roughness structure (cf. 13f) can also be seen in the small scan area of the AFM measurements.

The PSD functions calculated from the topography data and depicted in Figure 16, shows once again that the icephobic surface exhibits a higher roughness than the reference surface with the commercial coating in the investigated spatial frequency range. Especially in the range around a spatial frequency of 10 μm^{-1}, the PSDs of both functions differ significantly because of the spherical nanoroughness of the new multifunctional coatings.

The wetting parameter K_B was subsequently calculated from the PSDs to 0.14 for the reference sample surface and to 0.30 for the icephobic sample. These values confirm the results of the wetting analysis at the beginning of this section: The commercial coating with a contact angle of about 48° exhibits a surface structure with a K_B value clearly below the necessary criterion for super-hydrophobicity. But for the icephobic one, the necessary criterion for super-hydrophobicity with $\kappa_B = 0.3$ is reached. Thus, the special roughness characteristic of this surface enables the observed hydrophobic properties and hence the improved icing behavior compared to the reference sample surface.

Taking SEM images and PSD analysis into account, it is possible to conclude that a hierarchical structure is obtained, similar to those present in nature such as lotus leaf. This hierarchical structure allows the coating to have stable super hydrophobic properties. In summary, the observed nanoroughness (spherical shapes) of the icephobic sample surface promotes the entrapment of air or vapor within the micro and nanofeatures and the wetting of such surface is predicted by Cassie-Baxter wetting model. In particular, the droplet touches only the crests of the roughness and air pocket remains entrapped between the droplet and the surface.

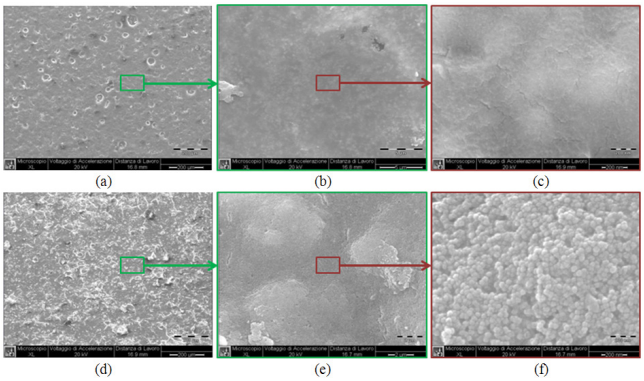

Figure 13: (a) reference sample surface, magnification 300X. (b) reference sample surface, magnification 10.000X. (c) reference sample surface, magnification 150.000X. (d) icephobic sample surface, magnification 300X. (e) icephobic sample surface, magnification 10.000X. (f) icephobic sample surface, magnification 150.000X. It is evident the hierarchical structure of the icephobic coating. A micro-features are well visible in the Figures (d) and (e) and in the Figure (f) the nano-features are evident.

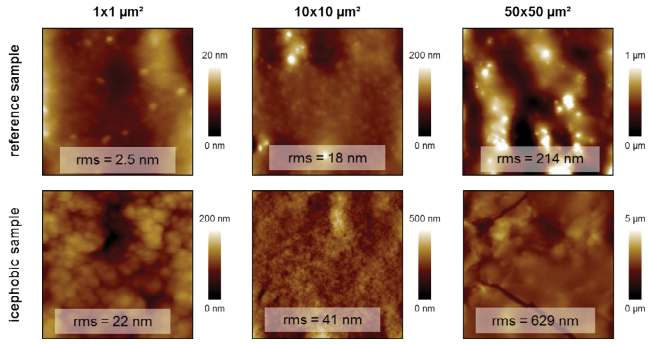

Figure 14: AFM topographic images and rms values of reference sample surface (1st line) and icephobic sample surface (2nd line).

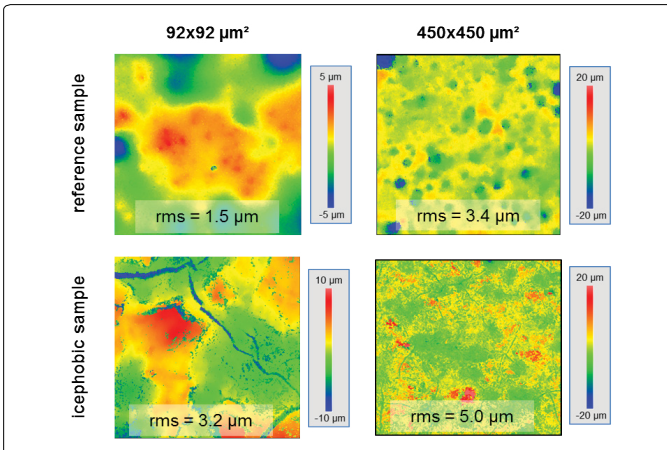

Figure 15: LSM topographic images and rms values of reference sample surface (1st line) and icephobic sample surface (2nd line).

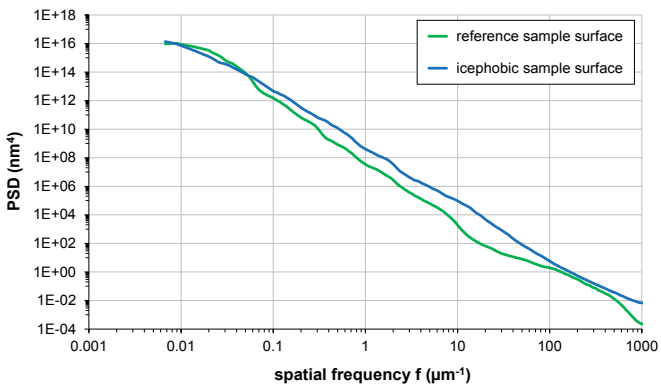

Figure 16: PSD functions of reference sample surface (green curve) and icephobic sample surface (blue curve).

Even if the morphological aspect is extremely important to have super-hydrophobicity and icephobicity, it is also important to preserve it for the entire cycle of flight from one maintenance and other of the aircraft. For this reason, it is important to evaluate the mechanical properties of the new coating. As described in the previous work [28] the main mechanical properties of the new multifunctional coating are the same or higher than the commercial one. The same consideration can be done also for the resistance to the hydraulic fluids [28].

Before scaling up this technology in relevant environment, the dynamic analysis at lab scale of the impingement of the microdroplets on the surface of both coatings was done. Tests showed clearly the different behavior of the surfaces. In fact as described in Figure 17a the water microdroplets that fall down on the commercial coating are well adherent with the surface and passing the time, they pile up until to create a one large macrodroplet. It is interesting to see in Figure 17a the large contact area between water droplet and surface.

On the contrary the new multifunctional coating with icephobic properties showed a complete different behavior. In fact in Figure 17b are reported the same instant times of those described previously for the commercial coating. The single water droplet, that falls down onto the surface, bounces from the surface, therefore there isn't accumulation of droplets. In particular in Figure 17b three different phases of droplet-surface interaction are evident:

The impact

It is evident the super-hydrophobic behavior of the surface analyzing the water droplet during the impact. No water spreading is evident and the droplet remains with a spherical shape.

The sliding

Once that the water droplet touches the surface, it slides on the surface due to the poor adhesion between water and material surface. As described previously, the work of adhesion of the new coating is 92% lower than the commercial one. This is corroborating experimentally from this test.

The sloshing and spinning

Once that the water droplet bounces from the surface, it starts to slosh and to spin far from the surface.

The new multifunctional coating showed also high resistance to harsh conditions as confirmed by the environmental test. In fact, compared with the commercial one (that is already certified), the behavior of the new coating was the same. In fact the visual inspection before and after the test, demonstrated that the new multifunctional coating preserves the aesthetical aspect and blistering; color changes and delamination are not present (Figures 18a-18d).

For a profound determination of the coating quality after the environmental test, analyses using optical microscopy were performed. As showed in Figures 19a-19d no cracks or in homogeneities are present on the surfaces of both coatings at microscopic level; in fact they are homogenous.

Finally in order to evaluate possible reduction of the adhesion between coating and substrate due to the infiltration of the humidity at the interface, cutting and tape test was performed on both coating.

The test confirmed the results reported in the previous work [28]. The new multifunctional coating showed an hardness higher than the commercial coating, in fact, as shown in the Figures 20a-20d, the blades of cutter failed to damage the surface of the new coating, only a few scratches are evident. On the contrary on the surface of the commercial coating, all scratches are well evident (Figure 20d). In

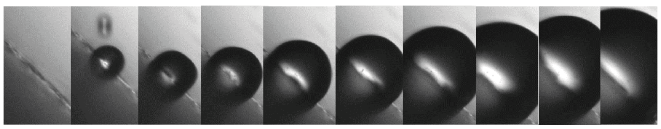

Figure 17a: Water droplets impingement on commercial coating.

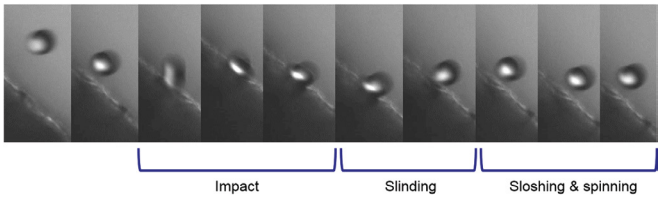

Figure 17b: Water droplets impingement on new multifunctional coating.

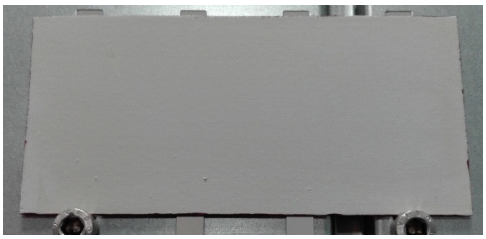

Figure 18a: New multifunctional coating before the test.

Figure 18b: New multifunctional coating before the test.

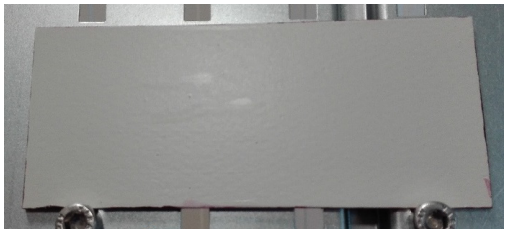

Figure 18c: Commercial coating before the test.

Figure 18d: Commercial coating after the test.

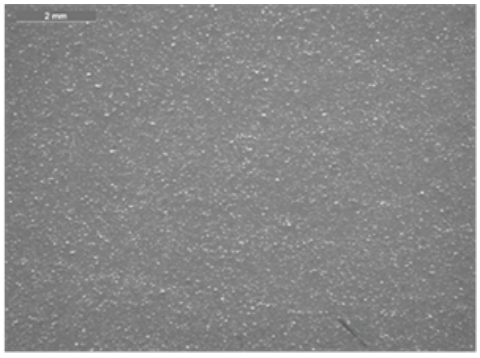

Figure 19a: Commercial coating - magn. 25X.

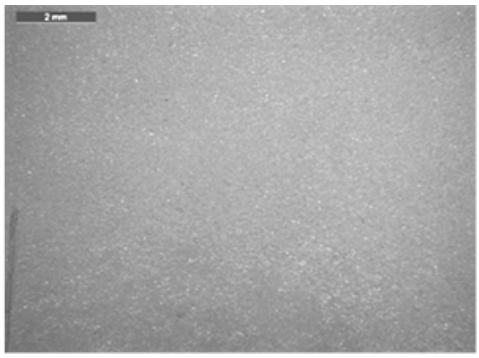

Figure 19b: Icephobic coating - magn. 200X.

any cases after the complete procedure of the test (in accordance with ASTM D 3359-2) the classification for both coatings was 5B. Therefore no reduction of the adhesion between coating and substrate is evident after environmental test.

The IWT tests demonstrated, in relevant environment, the effective reduction of accreted ice on the new multifunctional coating starting from the leading edge respect to the commercial one. This statement confirms the icephobic properties of the new coating.

The reduction of the accreted ice was measured through the length of compact ice that is accreted starting from the leading edge as reported in the sketch in Figure 21.

Figures 22a and 22b show the original images of the accreted ice in the region of the leading edge obtained respectively on commercial coating and new multifunctional coating. Whereas the Figures 22c and 22d represent the same images but after image analysis in order to optimize and to maximize the contrast with the aim to highlighted the accreted ice.

It is evident that the development of accreted ice (starting from the leading edge) is higher on the commercial coating respect to the

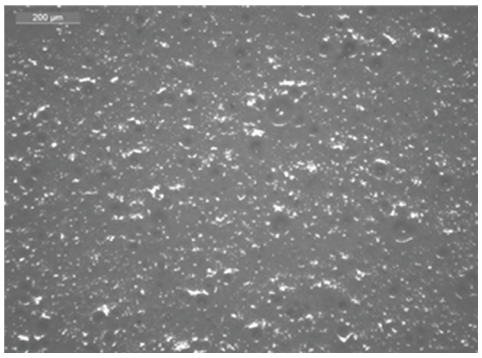

Figure 19c: Commercial coating - magn. 200X.

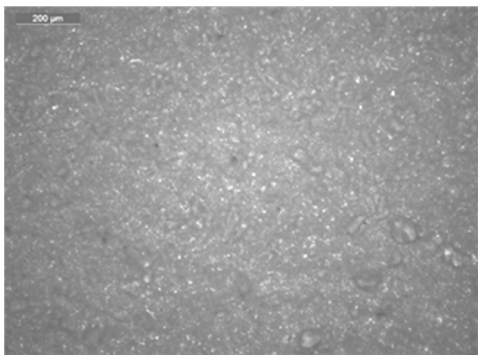

Figure 19d: Icephobic coating - magn. 200X.

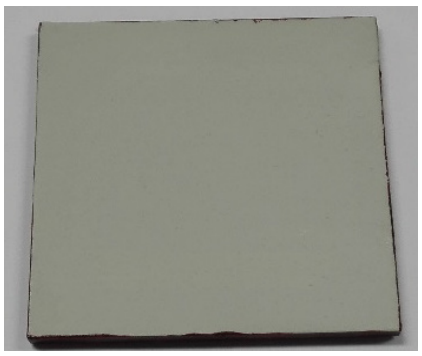

Figure 20a: New multifunctional coating before cutting and tape test.

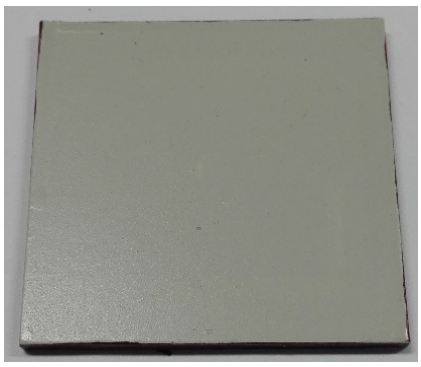

Figure 20b: Commercial coating before cutting and tape test.

Figure 20c: New multifunctional coating after cutting test.

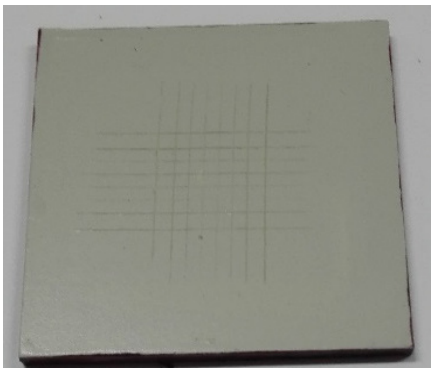

Figure 20d: Commercial coating after cutting test.

new multifunctional coating with icephobic property. This confirms the effectiveness of the new formulation and its functional property (icephobicity).

It is also interesting to study the type of accreted ice on the two airfoils, in fact in both cases the accreted ice is rime; in addition, the commercial coating shows also feathers developed on the final part of the compact accreted ice region. These feathers are not present on the new multifunctional coating.

Differences on a development of the accreted ice are mainly due to the icephobic property of the new formulation that in general delays the nucleation and growth of the ice (corroborating the effectiveness of the new coating). In addition, after all tests the manual strength necessary to remove the ice on the two airfoils is lower for the airfoil with new icephobic coating respect to the commercial one. This qualitative result corroborate the weak adhesion between ice and surface demonstrated quantitatively during the lab test (reduction of the work of adhesion between iced water droplet and surface of 92% respect to the commercial coating) and FEM analysis. This means that, combining passive icephobic systems with active de-icing systems, the ice is removed easier than the classical coating. It should also be considered that the wings of the aircrafts are in the airflow consequently, using a small energy from the airflow, the ice detaches from the surface; it go away from the components.

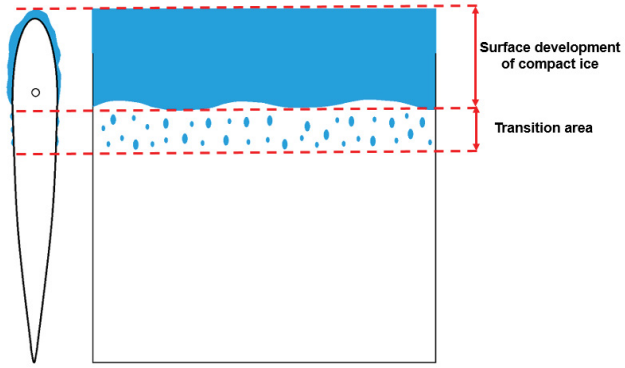

Figure 21: Sketch of the airfoil (side-view and on-top view) with the surface development of compact ice and the transition area.

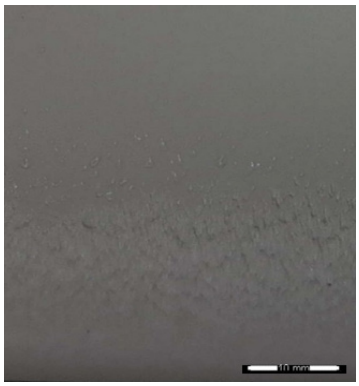

Figure 22a: Accreted ice on the commercial coating (original image).

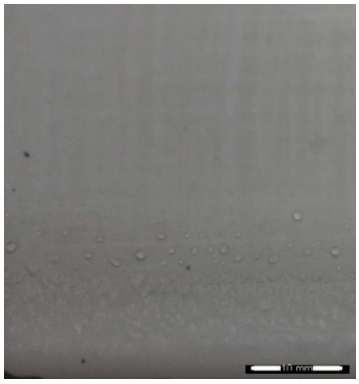

Figure 22b: Accreted ice on the new multifunctional coating (original image).

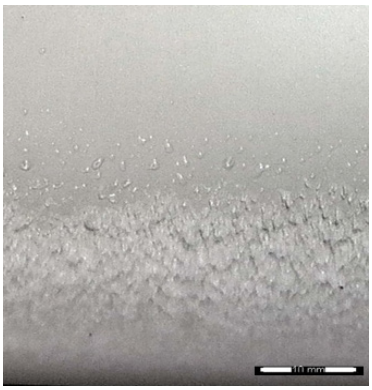

Figure 22c: Accreted ice on the commercial coating (after image analysis through DCE (Differential Contrast Enhancement filter).

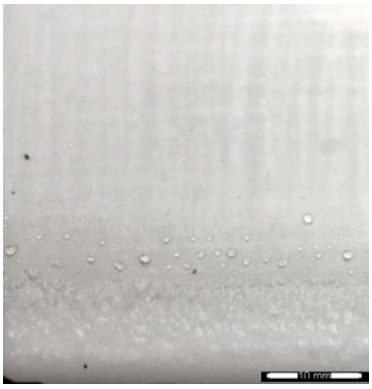

Figure 22d: Accreted ice on the new multifunctional coating (after image analysis through DCE (Differential Contrast Enhancement filter).

It is also interesting to analyze the transition region (as reported in the sketch of Figure 21) of the two airfoils in Figures 22a-22d. In fact on the commercial coating the transition area is wider than the new coating formulation and the freezed water droplets are numerically greater and more spread respect to the new multifunctional coating. In fact it is evident that the new coating shows a few droplets in a very short transition region and in addition they are freezed in a most spherical shape. It is highlighted that the points in which these droplets are present, are points in which the surface roughness is changed or it has surface defects and in these points happens that supercooled water droplet start to begin ice. Even if the water droplets have a spherical shape, the Cassie-Baxter condition is no longer maintained, in fact probably the Wenzel regime acts in this points. This is due to the local deterioration of the coating. In fact it is necessary to highlight that the most exposed area of the airfoil to the airflow, and consequently to the water impingement, is the leading edge. Therefore the leading edge is undergone to deterioration phenomena (rain, insects, sand, erosion phenomena) respect to the other part of the airfoil. For this reason the wings of civil aircrafts the leading edges are realized with naked (uncoated) metal. On the contrary the remaining parts of the wings are coated.

These results are obtained for all tests performed in the IWT and they confirm the statements reported above; a further test is represented in Figure 23 where the drastic reduction of the accreted ice on the new multifunctional coating with icephobic property is evident. Anyway to summarize the results of all tests, the bar-chart in Figure 24 is reported.

The value of accreted ice of the test 2 is not available, because during the measurements, the ice was broken and detached from the surface (further attestation of the very low adhesion between the ice and the new multifunctional coating).

Beyond the test 2, it is evident that the surface development of compact accreted ice is higher in case of commercial coating respect to the icephobic one. This statement corroborates the efficiency of the icephobic coating.

In all tests the development of accreted ice of the icephobic coating is 50% lower than the commercial coating.

Test 5 was performed using the same process parameters of test 1 in order to study the repeatability. It is evident a reduction of accreted ice on both coatings (commercial and new coating). This is due to the erosion phenomena at the leading edge and in particular on the stagnation point for both coatings. The accreted ice on new coating of the test 5 was reduced respect to the test 1; this means that the icephobic properties are improved during the utilization.

The reduction of accreted ice was reached also for commercial coating as demonstrate making a comparison between test 1 and test 5. In this case, the deterioration phenomena increase the roughness of the commercial coating giving hydrophobicity and consequently a small quantity of supercooled water droplets remain adherent on the surface.

Another way to determine the effectiveness and efficiency of the new multifunctional coating with icephobic property was to correlate the main IWT process parameters with the accreted ice for both types of airfoils (Figures 25a-25c).

In particular a correlation between altitude, MVD and LWC with accreted ice of two airfoils are plotted. It is clearly evident that the spatial distribution of the experimental points relative to the two airfoils is the same but the points of new multifunctional coating with icephobic property are shifted on the left. This gap gives an estimation of the effectiveness and efficiency of the icephobicity. As bigger the gap, the greater is the icephobicity.

Conclusions

In this work a further development of the new multifunctional aeronautical coating with aesthetic and icephobic properties were described.

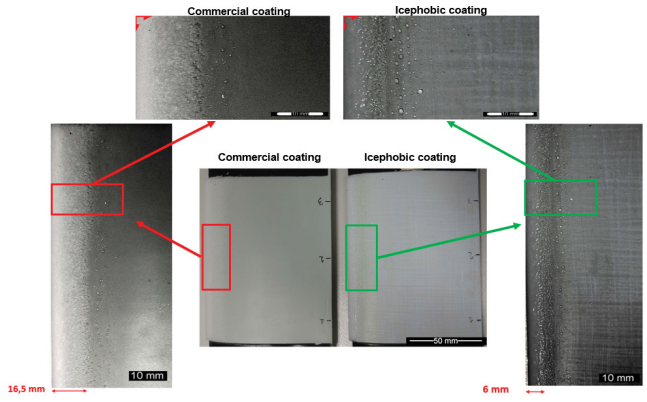

Figure 23: Comparison of the different accreted ice (at different magnification) on the two airfoils with new multifunctional coating and the commercial one. It is evident a drastic reduction of the ice accreted starting from the leading edge of the new coating respect to the commercial coating.

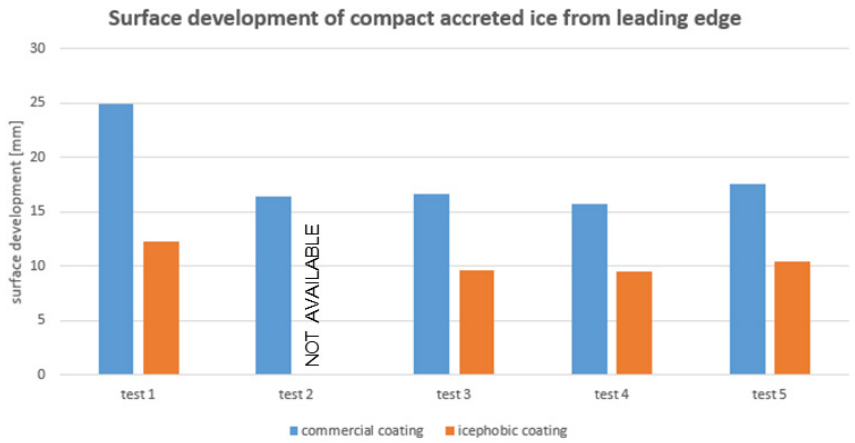

Figure 24: Comparison of the accreted ice on the two coatings for all tests performed in the IWT.

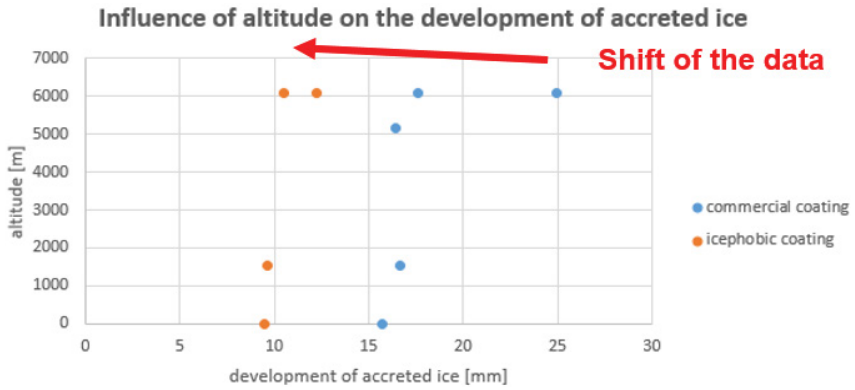

Figure 25a: Correlation between accreted ice of the two coatings respect to the altitude simulated in the IWT.

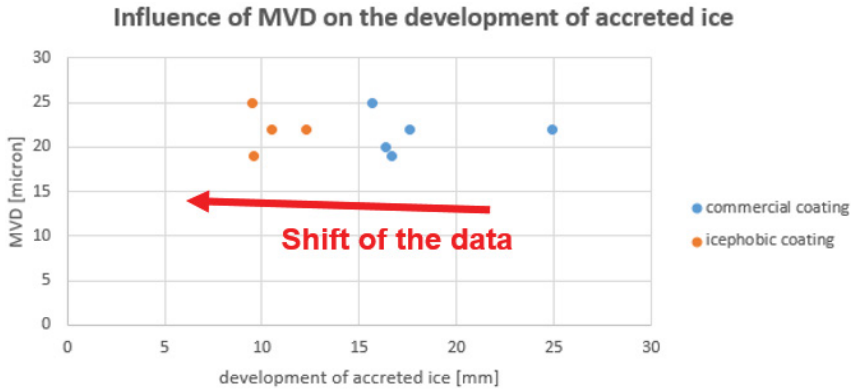

Figure 25b: Correlation between accreted ice of the two coatings respect to the MVD simulated in the IWT.

Once design and realized at lab scale, the new multifunctional coating was tested at lab scale with the aim to check the new icephobic property. Subsequently a deep analysis of the morphology was done with the aim to investigate the reason for the improved icephobicity. It has been shown that spherical nano roughness seen for the novel icephobic coating enables the special functionalities.

The characterization at lab scale reported in this work supplements the results obtained in the previous work, corroborating the high quality of the new coating. In fact the new coating formulation passes all standard tests performed until now. In particular, the new multifunctional coating passes also the test of long-time exposure in high concentration of relative humidity similar to the commercial one.

The different behavior of the liquid droplets during the impingement onto the sample surfaces was described through dynamic characterization at lab scales. It is clearly evident the behavior of the new coating and in particular its super-hydrophobic property. The

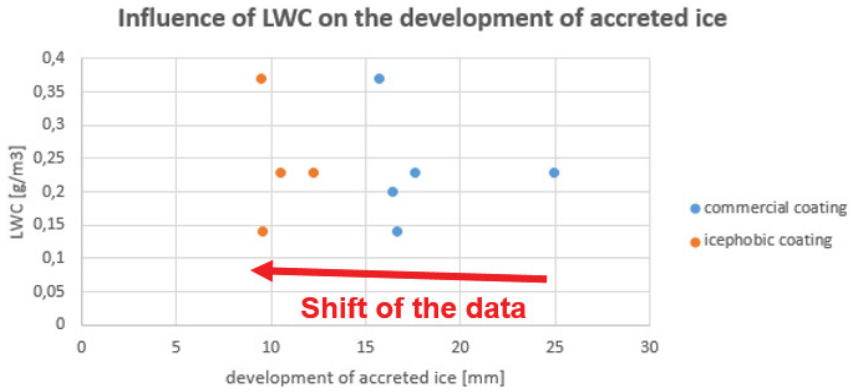

Figure 25c: Correlation between accreted ice of the two coatings respect to the LWC simulated in the IWT.

dynamics of interaction between droplet and surface are completely different respect to the commercial coating.

A further issue reported in this work was also to scale up this new coating formulation in relevant environment in order to verify the icephobic property. For this reason symmetric NACA 0015 airfoils were realized using 3D printing technology which were afterwards coated with the commercial coating (to use as reference) and the new multifunctional coating. Results after Icing Wind Tunnel tests were very encouraging, in fact without using active de-icing systems the reduction of accreted ice on the new multifunctional coating was of 50% respect to the commercial one.

Future activities will be addressed to complete the characterization of the new multifunctional coating and to test this passive anti-icing system with one or more active de-icing technologies.

Acknowledgement

Author would like to thank to Ottavio Minieri for the support during the IWT tests.

References

1. Murphya C, Wallace S, Knight R, Cooper D, Seller T (2015) Treatment performance of an aerated constructed wetland treating glycol from de-icing operations at a UK airport. Ecological Engineering 80: 117–124.
2. Gray L (2013) Water pollution prevention and control report. Review of aircraft deicing and anti-icing fluid storm water runoff control technologies. MANE 6960H01.
3. Sulej M, Palkowska Z, Namieśnik J (2012) Contaminants in airport runoff water in the vicinities of two international airports in Poland. Pol J Environ Stud 21: 725–739.
4. Thomas SK, Cassoni RP, MacArthur CD (1996) Aircraft anti-icing and de-icing techniques and modeling. J Aircraft 41: 1291–1297.
5. Falzon BG, Robinson P, Frenz S, Gilbert B (2015) Composites: Part A, 68: 323–335.
6. Boinovich LB, Emelyanenko AM (2013) Anti-icing potential of super hydrophobic coatings. Mendeleev Commun 23: 3-10
7. Boinovich L, Emelyanenko AM, Korolev VV, Pashinin AS (2014) Effect of wettability on sessile drop freezing: When super hydrophobicity stimulates an extreme freezing delay. Am Chem Soc 30: 1659-1668
8. Makkonen L (2013) Ice adhesion- theory measurements and countermeasures. J Adh Sci and Tech 26: 413-445.
9. Susoff M, Siegmann K, Pfaffenroth C, Hirayama M (2013) Evaluation of icephobic coatings-Screening of different coatings and influence of roughness. App Surf Sci 282: 870-879.
10. Momen G, Farzaneh M (2014) Facile approach in the development of icephobic hierarchically textured coatings as corrosion barrier. App Surf Sci 299: 41-46.
11. Strobl T, Storm S, Kolb M, Haang J, Hornung M (2014) Development of a hybrid ice protection system based on nanostructured hydrophobic surfaces. Proc. 29th Congress of the International Council of the Aeronautical Science St. Petersburg Russia.
12. Lazauskas A, Guobiene A, Prosycevas I, Baltrusaitis V, Grigaliunas V, et al. (2013) Water droplet behavior on super hydrophobic SiO_2 nanocomposite films during icing/deicing cycles. Materials char. 82: 9-16.
13. Zhu L, Xue J, Wang Y, Chen Q, Ding J, et al. (2013) Ice-phobic coatings based on silicon-oil-infused polydimethylsiloxane. Appl Mater Inter 5: 4053–4062.
14. Attinger D, Frankiewicz C, Betz AR, Schutzius TM, Ganguly R, et al. (2014) Surface engineering for phase change heat transfer: A review. MRS Energy & Sustainability Materials Research Society 1: 1-40.
15. Laforte C, Blackburn C, Perron J (2015) A review of ice-phobic coating performances over the last decades. SAE Technical paper 01: 2149.
16. Saito H, Takai K, Yamauchi G (1997) A study on ice adhesiveness to water-repellent coating. Mater Sci Res Int 3: 185–189.
17. Kulinich SA, Farzaneh M (2009) Ice adhesion on super-hydrophobic surfaces. App Surf Sci 255: 8153–8157.
18. Kulinich SA (2011) Super hydrophobic surfaces: are they really ice-repellent? Langmuir 27: 25–29.
19. Riosa PF, Dodiukb H, Kenigc S, McCarthyd S, Dotan A (2007) The effect of polymer surface on the wetting and adhesion of liquid systems, J. Adh. Sci. Tech. 21: 227-241.
20. Varanasi KK (2010) Frost formation and ice adhesion on super hydrophobic surfaces. App Phys Let 97: 23.
21. Etzler FM (2003) Contact angle wettability and adhesion. 3 KL Mittal (Ed.) VSP Utrecht.
22. Mittal KL (2013) Advances in contact angle. Wettability & Adhesion. Scrivener Publishing, Willey.
23. Meuler AJ (2010) Relationships between water wettability and ice adhesion. ACS App Mat Inter 2: 3100–3110.
24. Farhadi S, Farzaneh M, Kulinich SA (2011) Anti-icing performance of super hydrophobic surfaces. App Sur Sci 257: 6264–6269.
25. Jung S (2011) Are super hydrophobic surfaces best for icephobicity? Langmuir 27: 3059–3066.
26. Hassan MF, Lee HP, Lim SP (2010) The variation of ice adhesion strength with substrate surface roughness. Meas Sci Tech. 21: 7.
27. Bascom WD, Cottingt RL, Singlete CR (1969) Ice adhesion to hydrophilic and hydrophobic surfaces. J.Adhes 1: 246.
28. Mazzola L (2016) Aeronautical livery coating with icephobic property. J Surface Engineering 32: 733-744.
29. Flemming M, Duparré A (2006) Design and characterization of nanostructured ultrahydrophobic coatings. Appl Opt 45: 1397-1401.
30. Flemming M, Coriand L, Duparré A (2009) Ultra-hydrophobicity through

stochastic surface roughness in: Superhydrophobic Surfaces. CRC Press Boca Raton FL: 19-38.

31. Jones RAL, Richards RW (2006) Polymers at surface and interfaces. Cambridge University Press.
32. Owens DK, Wendt RC (1968) Estimation of the surface free energy of polymers. J Appl Polym Sci 13: 1741.
33. Zenkiewicz M (2007) Methods for the calculation of surface free energy of solids. Pol Test 26: 14-19.
34. Rudawska A, Jacniacka E (2009) Analysis of determining surface free Energy Uncertainty with the Owens-Wendt method. Inter J Adhes Adhes 29: 451-457.
35. Holysz L, Chibowski E, Terpilowsi K (2008) Contact angle wettability and adhesion, Leiden.
36. Duparré A, Coriand L (2013) Assessment criteria for superhydrophobic surfaces with stochastic roughness, in advances in contact angle, wettability and adhesion1. Wiley-Scrivener Beverly MA: 197-201.
37. Coriand L, Mitterhuber M, Duparré A, Tünnermann A (2011) Definition of roughness structures for superhydrophobic and hydrophilic optical coatings on glass. Appl Opt 50: C257-C263.
38. Duparré A, Ferré-Borrull J, Gliech S, Notni G, Steinert J, et al. (2002) Surface characterization techniques for determining rms roughness and power spectral densities of optical components. Appl Opt 41: 154-171.